Delineating Core and Surface State Heterogeneity in Carbon Dots during Electron Transfer

Umarfaruk S. Sayyad,[a] *Himanshu Bhatt,*[b] *Hirendra N. Ghosh,*[c] *Somen Mondal**[a]

[a]*Institute of Chemical Technology, Mumbai, Marathwada Campus, Jalna, Maharashtra 431203, India,*

[b]*Institute of Nano science and Technology, Mohali, Punjab 140306, India*

[c]School of Chemical Sciences, National Institute of Science Education and Research (NISER), Bhubaneswar, Odisha 752050, India

1 Material and Method

1.1 Material

Citric acid (Sigma Aldrich), urea (SDFCL), N, N- dimethyl formamide (DMF) and methanol (finar), 1,1 dichloromethane (Molychem), methyl viologen dichloride hydrate (sigma aldrich), n-Tetrabutyl ammonium perchlorate (thermo chemicals), triethanolamine (TEOA) (Molychem), and ethyl acetate, (Molychem). All experiments were carried out using ultrapure water and HPLC-grade solvents.

1.2 Synthesis of C-Dots

C-Dots were synthesized using the hydrothermal method with slight modifications of the previously reported method. [1,2] Briefly citric acid and urea (1 gm each) were dissolved in DMF (15 mL). The solution was transferred to the teflon lined autoclave and kept in the oven at 180 °C for 12 hours. The obtained brown crude product was filtered using Whatman filter paper to remove undesired solid particles. The filtrate was dried by using a rotary evaporator at 70 °C.

1.2.1 Purification of C-Dots

Purification of C-dots was done using column chromatography. The silica powder having mesh size 400-500 μm was used as a stationary phase and a mixture of DCM containing different percentages of methanol was used as a mobile phase. Samples were collected from

various bands separately. Initially, by eluting 100% DCM all agglomerates and fluorophores were collected and discarded. Then slowly the percentage of methanol was increased in the mobile phase then at 4-8% methanol pure blue emitting (B-C-Dots) were collected after increasing the concentration (12 to 15%) pure green emitting (G-C-Dots) and above 25% pure red emitting (R-C-Dots) C-Dots were collected. After the column, the eluent was evaporated using a rotary evaporator at 50°C and stored in a refrigerator.

1.3 Instrumentation and Characterization

1.3.1. Transmission Electron Microscopy and HRTEM Analysis:

The surface morphology and particle size analysis were measured using high resolution transmission electron microscope and images were captured using transmission electron microscopy using instrument modal JEOL JEM 2100 with an accelerating bias of 200 keV.

1.3.2. XPS analysis:

XPS measurements were performed on the K-Alpha X-ray Photoelectron Spectrometer (XPS) System of Thermo Fisher Scientific using an Al K micro focus monochromator. The variable operating energy (100-4000 eV) was used to record the spectrum.

1.3.3. Fourier Transform Infrared Spectroscopy:

JASCO FT/IR 6600 spectrometer was used to determine the Functional group presence on the surface of C-Dots on ATR mode at room temperature.

1.3.4. UV-Visible Spectra and PL Spectra:

To investigate the optical properties, the absorbance of all the C-Dots was measured on Shimadzu UV-2600i UV-Visible spectrophotometer, and steady state fluorescence spectra were recorded JASCO spectrofluorometer using HPLC grade water as a solvent.

1.3.5. Raman Spectroscopy:

Raman spectra of all C-Dots were captured using In Via Raman Microscope using excitation light source High Power Near IR Diode Laser, 300 mW at 785 nm (air cooled) integral narrow bandpass filter with external mounting on laser kinematic baseplate.

1.3.6. Time Correlated Single Photon Counting Measurement:

Time resolved fluorescence analysis was done using TCSPC mode using Delta pro TM-TCSPC lifetime system made by Horiba Scientific. The samples were excited using two different light sources 340 nm and 405 nm using a nano LED light source and the emission were monitored at 440 and 520 nm respectively. The instrument response function was recorded as 80 ps. Initially, the IRF was measured using a soap solution in water. All C-Dots were dissolved in water. The obtained data was fitted using the software EZ time.

$$\tau_{avg} = \sum \alpha_i \tau_i / \sum \alpha_i \quad \text{..... S1}$$

1.3.7. Experimental Setup of Femtosecond TA Spectroscopy:

Transient Absorption spectra were obtained using a HELIOS TA spectrometer from Ultrafast Systems. The laser system utilized a Spitfire Ace Ti: Sapphire amplifier by Spectra Physics. It was initially initiated by a Ti: Sapphire oscillator operating at 800 nm which has a pulse duration of 80 fs and repetition rate of 1 kHz. The output from the amplifier was divided into two beams: one served as a pump and the other probe. A portion of the regenerative amplifier output was directed through an optical parametric amplifier (TOPAS, by Light Conversion) to generate various needed wavelengths. These wavelengths were then introduced into the spectrometer with precise timing using a synchronized chopper, producing signals synchronized at 500 Hz. The path of the probe beam was directed through a computer-controlled delay stage and then through a CaF_2 (Calcium fluoride) crystal to create a white light continuum. All experiment data were subsequently analyzed using Surface Xplorer software. All transient absorption measurements were done using a quartz cell with a path length of 2 mm.

1.4. Electrochemical voltametric measurement:

To identify the valance band (HOMO) levels of C-Dots, the cyclic voltammetry experiment was performed using three electrode system where the glassy carbon electrode functionalized in 0.5 M sulfuric acid up to 50 cycles and cleaned by alumina slurry was used as a working electrode, the SCE containing 3M KCl as a supporting electrolyte was used as a reference and platinum wire as a counter electrode on Metrohm Autolab electrochemical workstation. Initially, 2 mg CQDs were dispersed in 70% isopropyl alcohol and water sonicated for 30 min to make the uniform ink, and the ink was drop cast on active GCE surface. After drying the WE the CV analysis was done in 0.05 M N-tetrabutyl ammonium perchlorate in ethyl acetate at a scan rate of 0.05 Vs^{-1}.

1.5. Measuring of Methyl viologen radical generation:

Here we measured the methyl viologen radical generation using B-C-Dots, G-C-Dots, and R-C-Dots after irradiation of UV and Visible light. First, 2 ml C-Dots solution (absorbance ~0.2) was added in.5 mM methyl viologen (MV^{2+}) solution, and 0.230 ml triethanol amine (TEOA) was mixed in the solution as a sacrificial electron donor in 3.5 ml cuvette and made it airtight. Then, N_2 was purged in the solution for 30 minutes to make the inert

atmosphere inside the cuvette exposed. After that, we measure the absorbance of the solution in 2-minute intervals after illumination of UV and Visible light. The yield of radical generation was negligible in the absence of an inert environment and sacrificial electron donor. All the control experiments were also performed by changing the conditions such as without TEOA, sacrificial electron donor, etc.

The concentration of radical generation was determined from the absorbance spectrum using Lambert Beer's equation. [3]

$$A = \varepsilon C l \text{ ----------} \quad S2$$

Where A is the absorbance of MV^{2+} radical at 605 nm, ε is the absorption coefficient of MV^{2+} (13700 M^{-1} cm^{-1}) [4], C is the concentration of solution and l is Path length (1 cm).

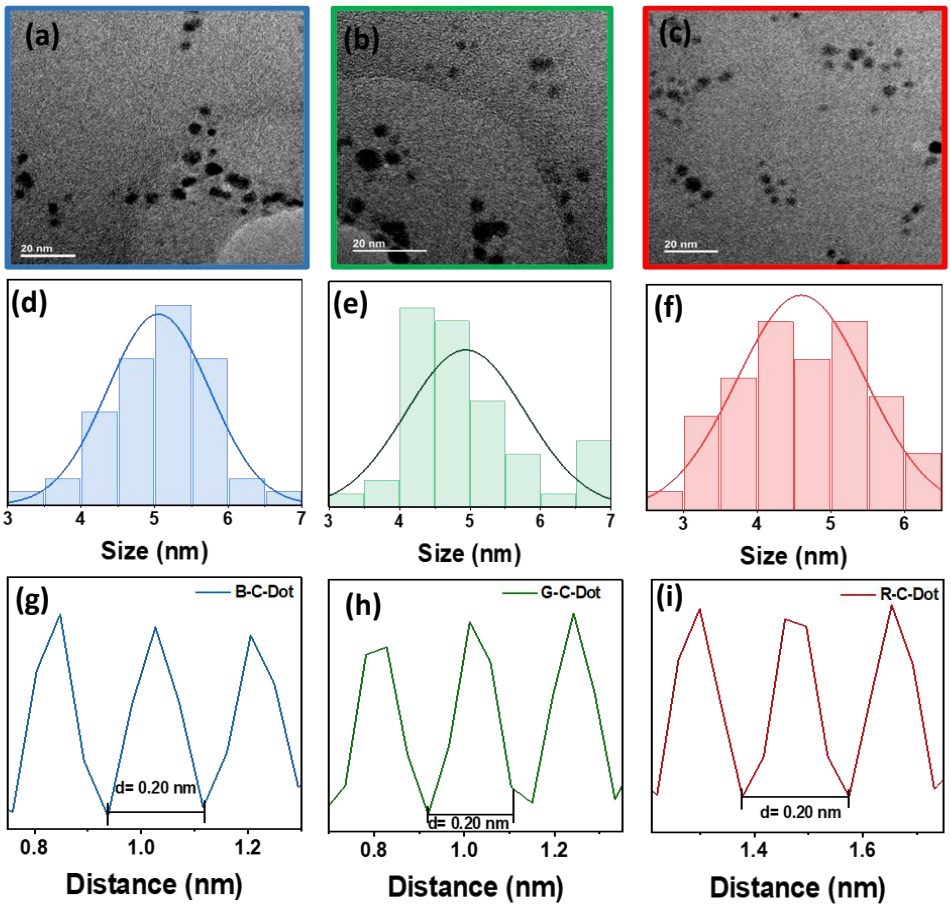

Figure S1: (a-c) Wide area TEM (d-e) images average particle Size distribution analysis and (d-f) HRTEM interplanar distance measurements for B-C-Dot, G-C-Dot, and R-C-Dot respectively.

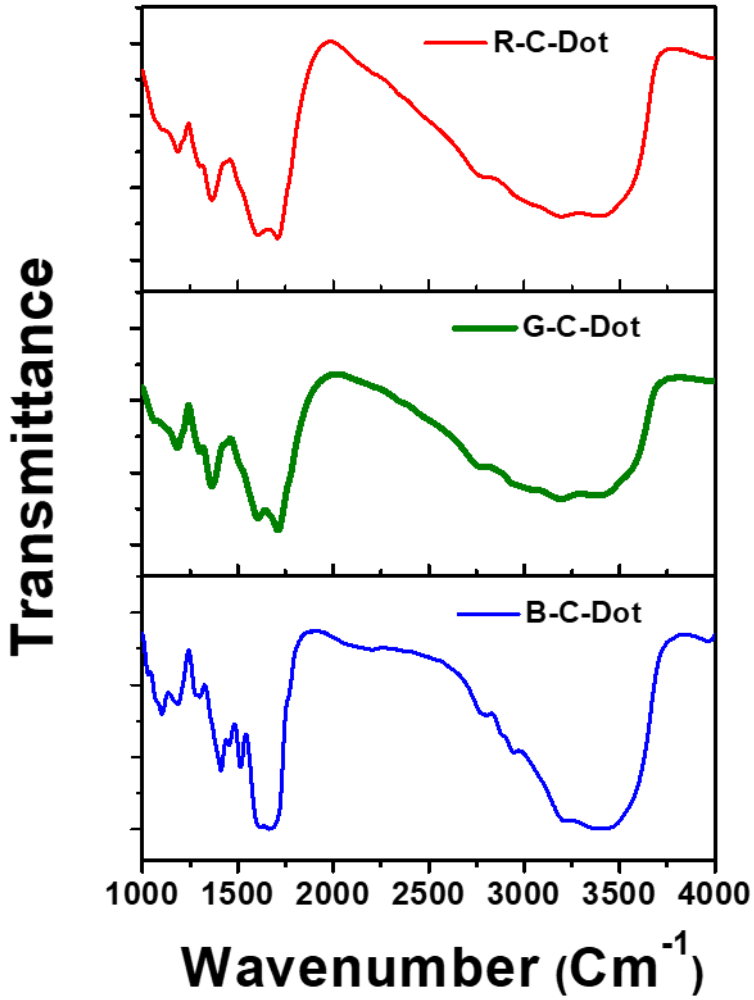

Figure S2: FTIR spectra of B-Cots, G-C-Dots and R-C-Dots

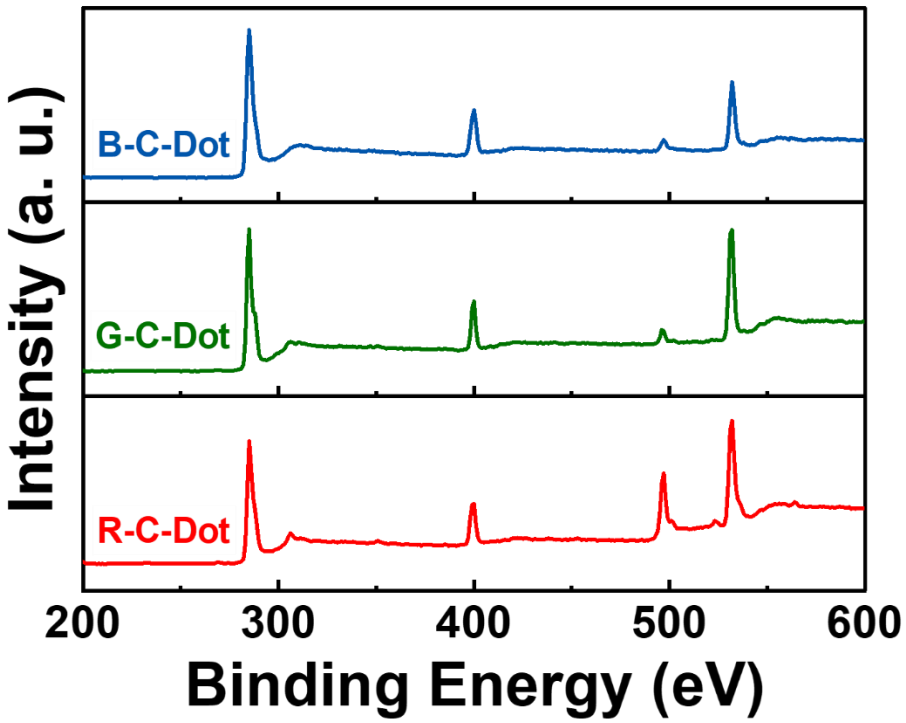

Figure S3: The full survey of XPS of the different C-Dots.

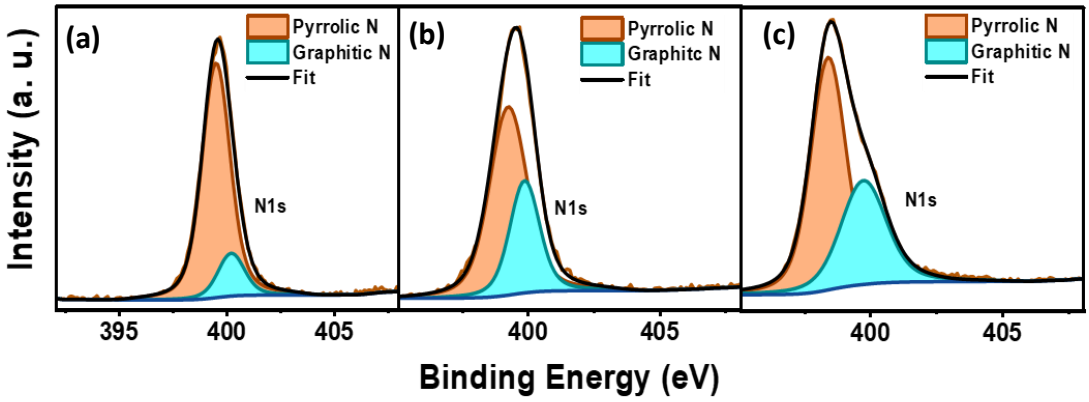

Figure S4: HRXPS N1s spectra of (a) B-Cots, (b) G-C-Dots, and (c) R-C-Dots.

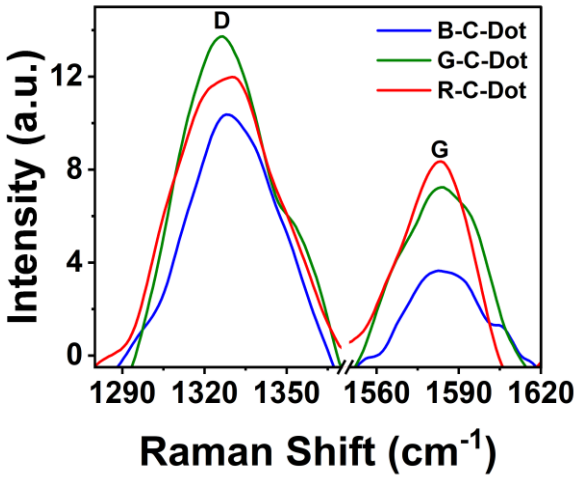

Figure S5: Raman spectra of the C-Dot using excitation 785 nm laser.

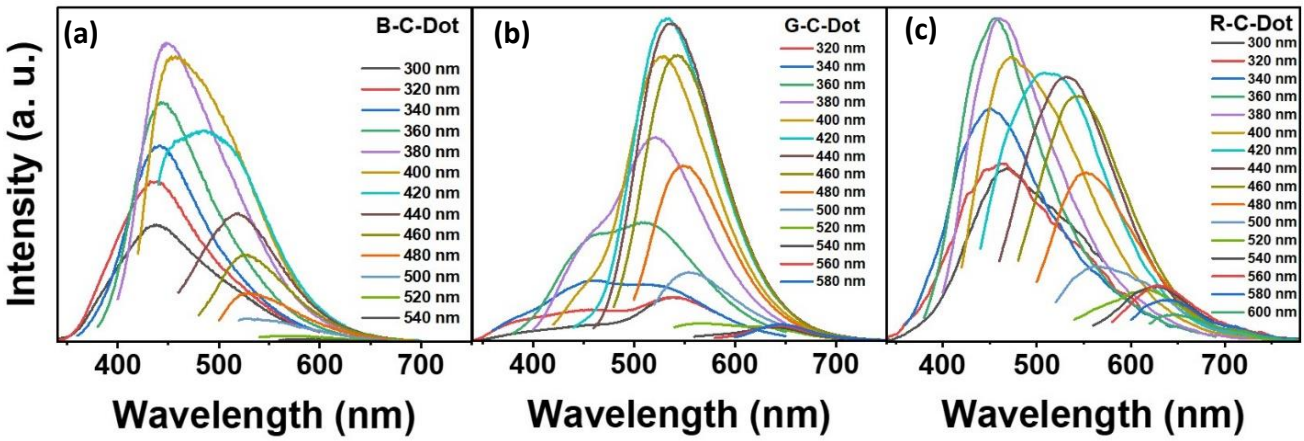

Figure S6: Excitation wavelength dependent steady state emission spectra of (a) B-C-Dot (b) G-C-Dot and (c) R-C-Dot.

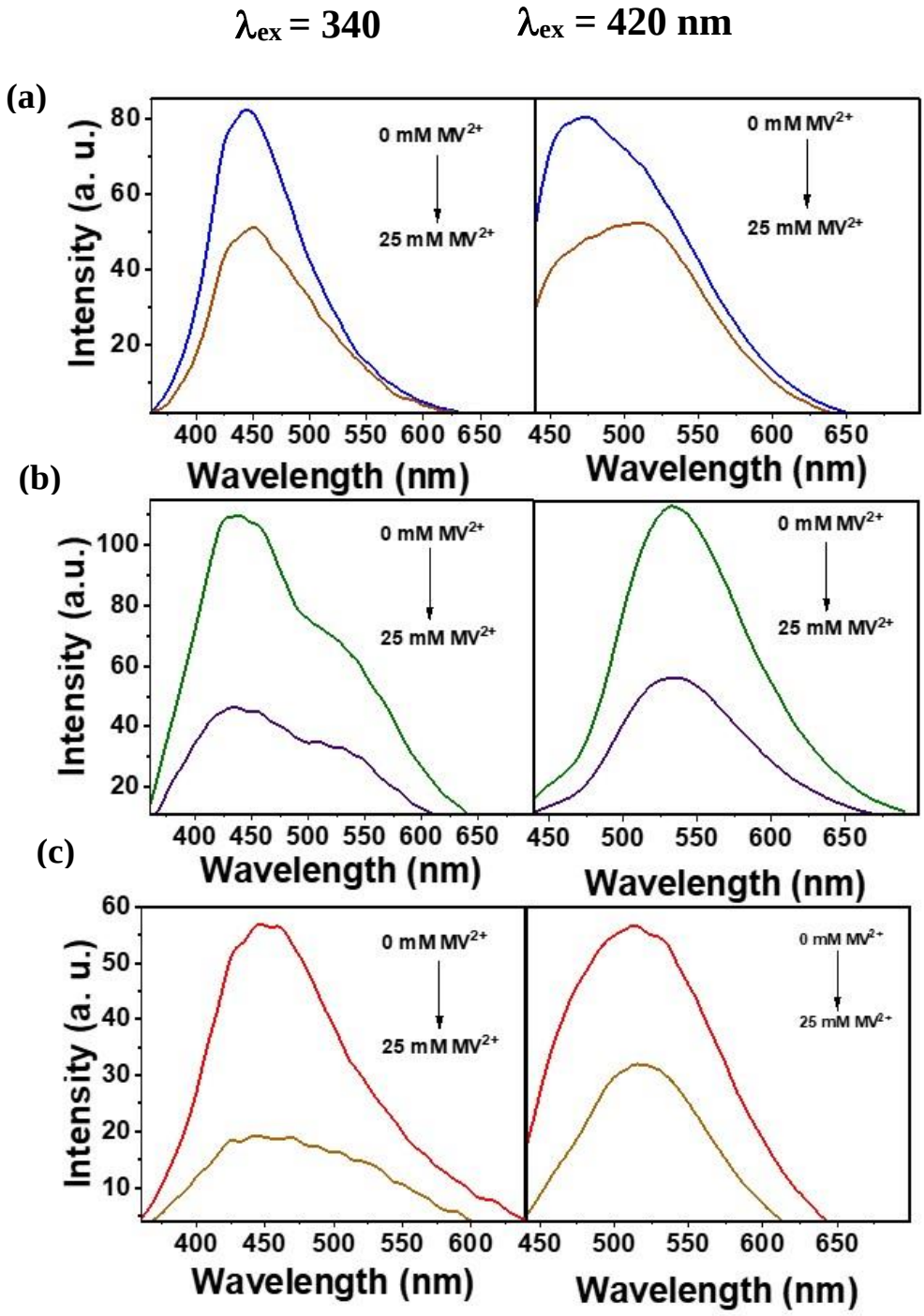

Figure S7: Steady state PL measurement of (a) B-C-Dots (b) G-C-Dots (c) R-C-Dots in the presence of different concentrations of MV^{2+} after the excitation of 340 and 420 nm.

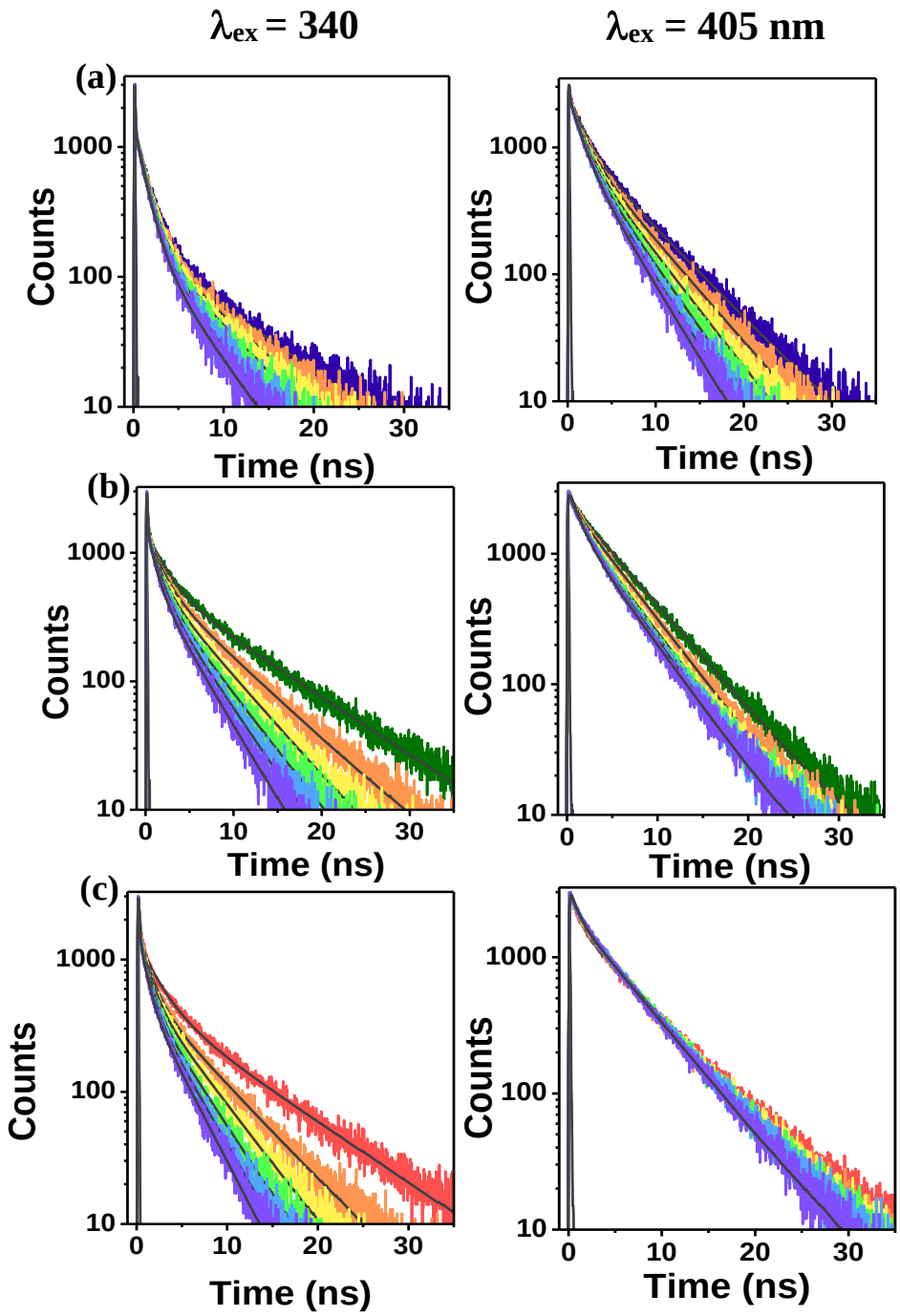

Figure S8: Time resolved PL measurement of (a) B-C-Dots (b) G-C-Dots (c) R-C-Dots in the presence of different concentrations of MV^{2+} after the excitation of 340 and 405 nm excitation.

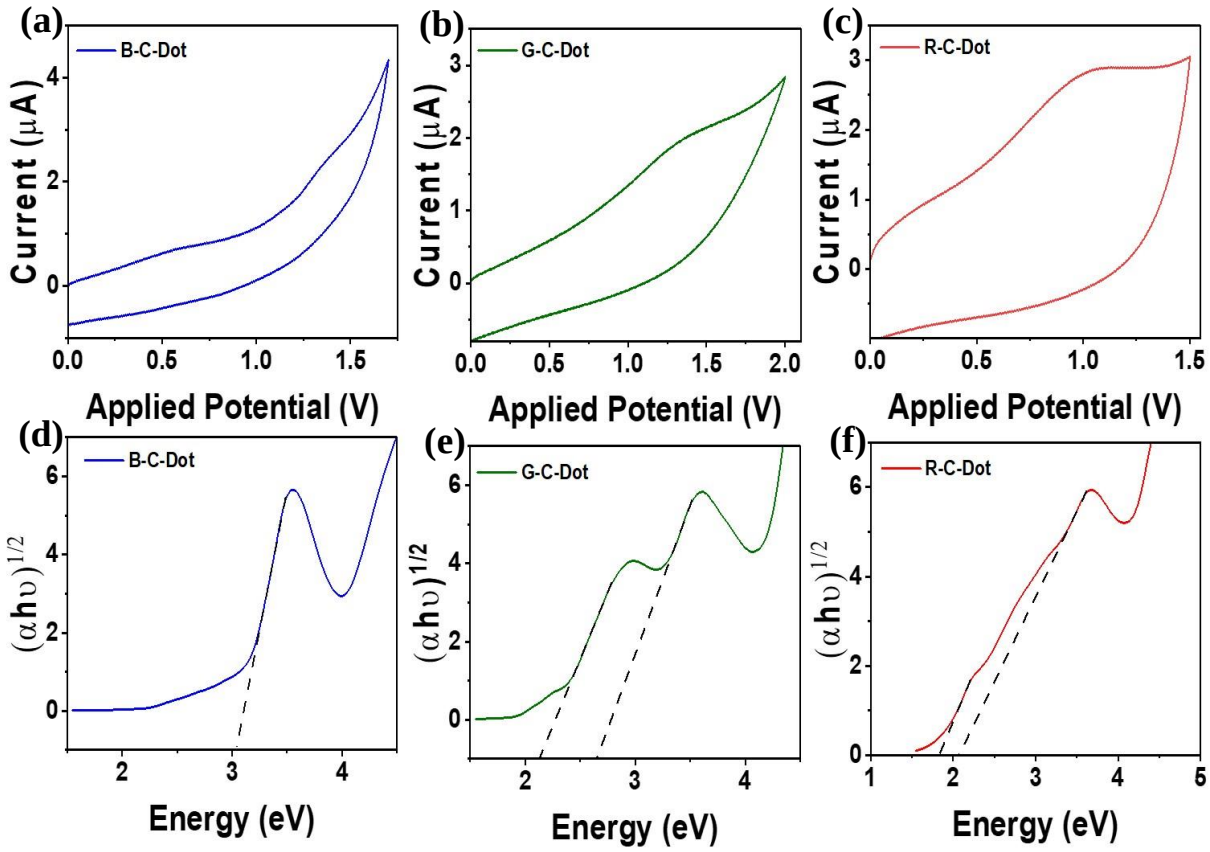

Figure S9: Cyclic Voltammetry (CV) curve (top panel) and tauc plot (bottom panel) for (a), (d) B-C-Dot, (b), (e) G-C-Dot, and (c), (f) R-C-Dot respectively.

The valance band (VB) is calculated from the oxidation potentials (E_{ox}) of the C-Dots of CV and the band gap is determined from the absorbance using the following relations:

$E_{HOMO} = - [E_{ox.} + 4.75]$ ---------- S_3

$E_g = 1240/\lambda_{onset}$ ---------- S_4

$E_{LUMO} = E_{HOMO} - E_g$ ---------- S_5

Where E_g is the band gap energy, λ_{onset} is the absorbance wavelength.

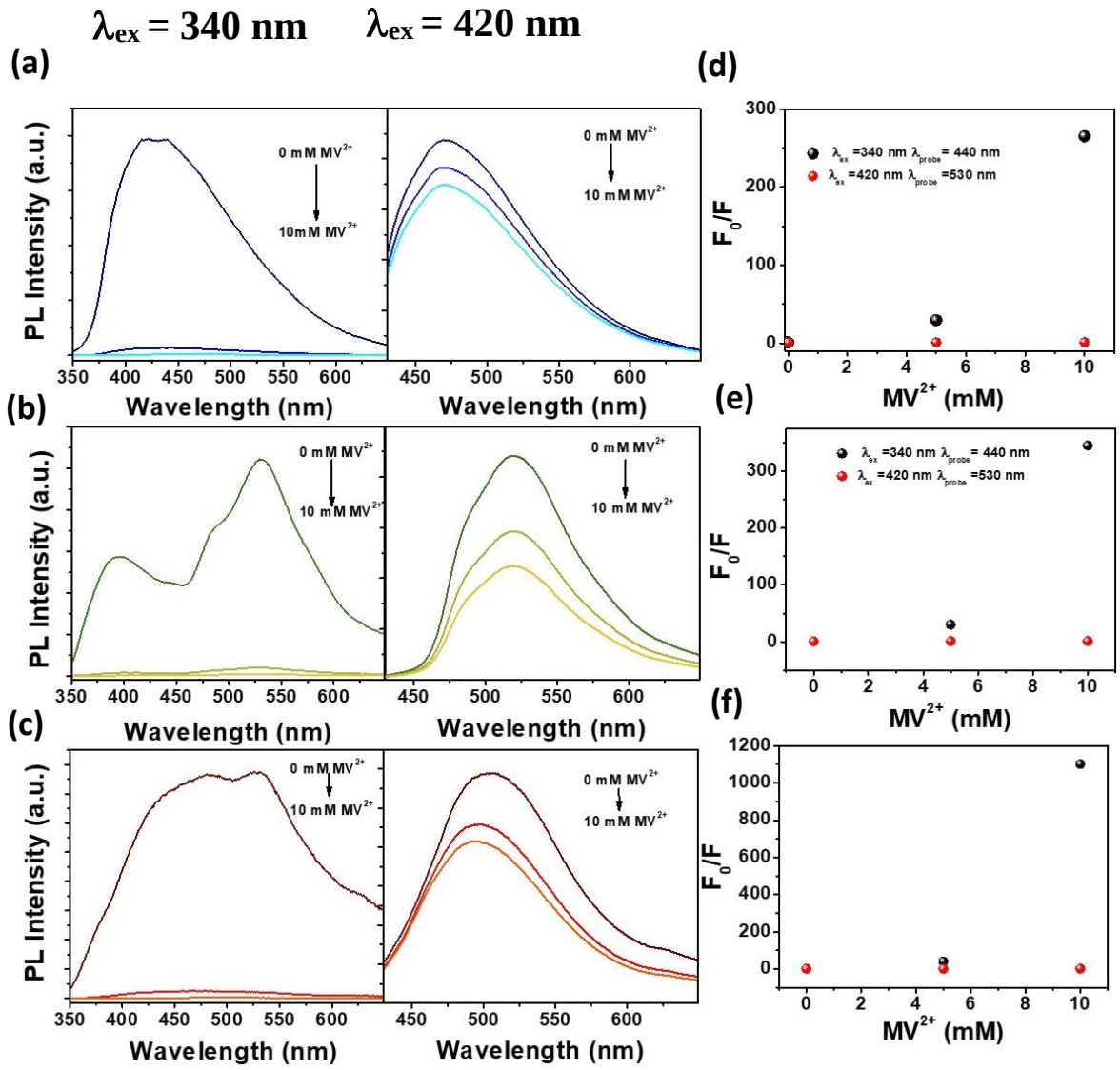

Figure S10: Steady state PL measurement of (a) B-C-Dots (b) G-C-Dots (c) R-C-Dots in the presence of different concentrations of MV^{2+} after the excitation of 340 and 420 in DMSO, Stern-Volmer quenching plots for (d) B-C-Dots (e) G-C-Dots (f) R-C-Dots in presence of different concentrations of MV^{2+} up to 10 mM.

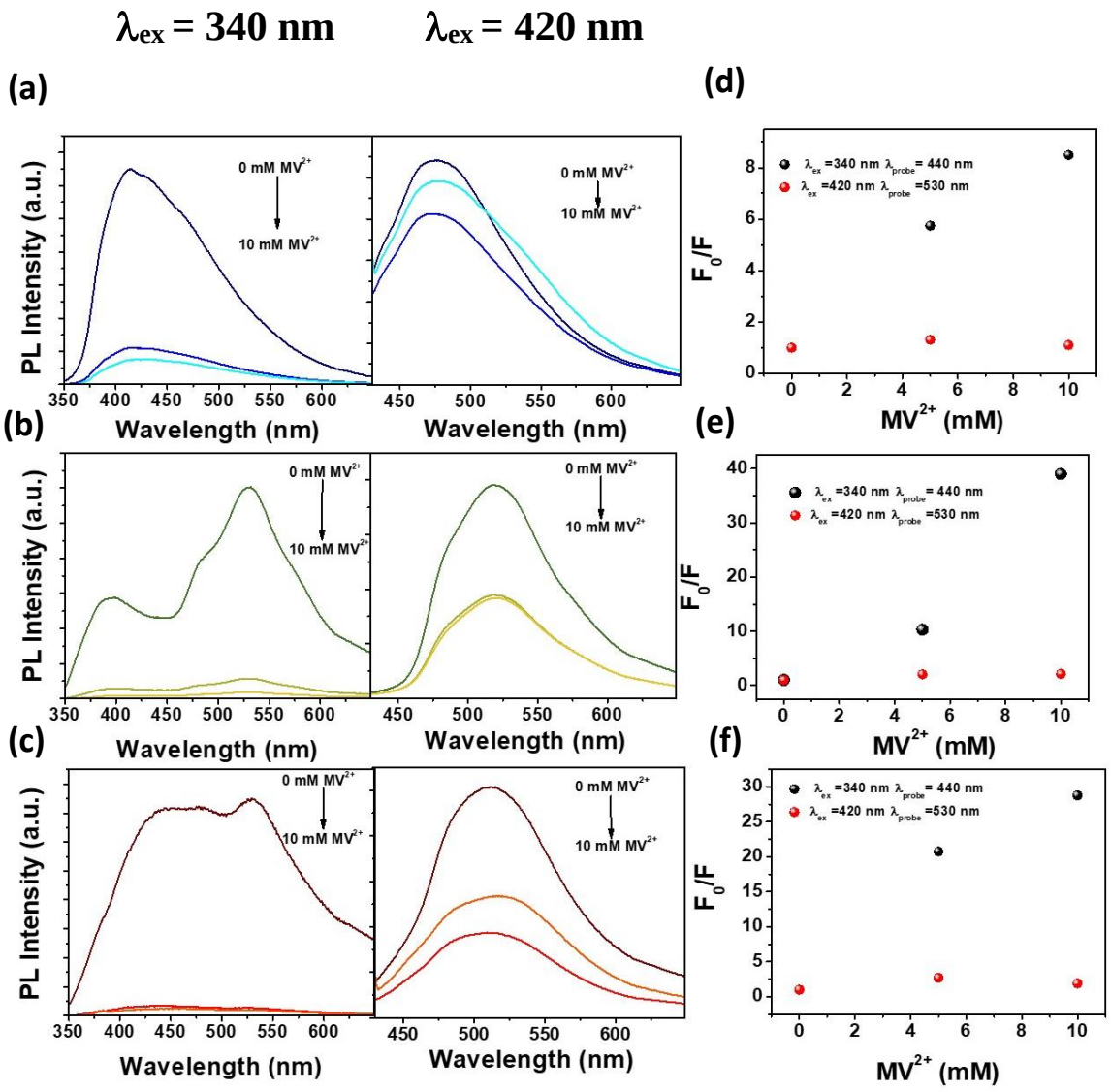

Figure S11: Steady state PL measurement of (a) B-C-Dots (b) G-C-Dots (c) R-C-Dots in the presence of different concentrations of MV^{2+} after the excitation of 340 and 420 in DMF, Stern-Volmer quenching plots for (d) B-C-Dots (e) G-C-Dots (f) R-C-Dots in presence of different concentrations of MV^{2+} up to 10 mM.

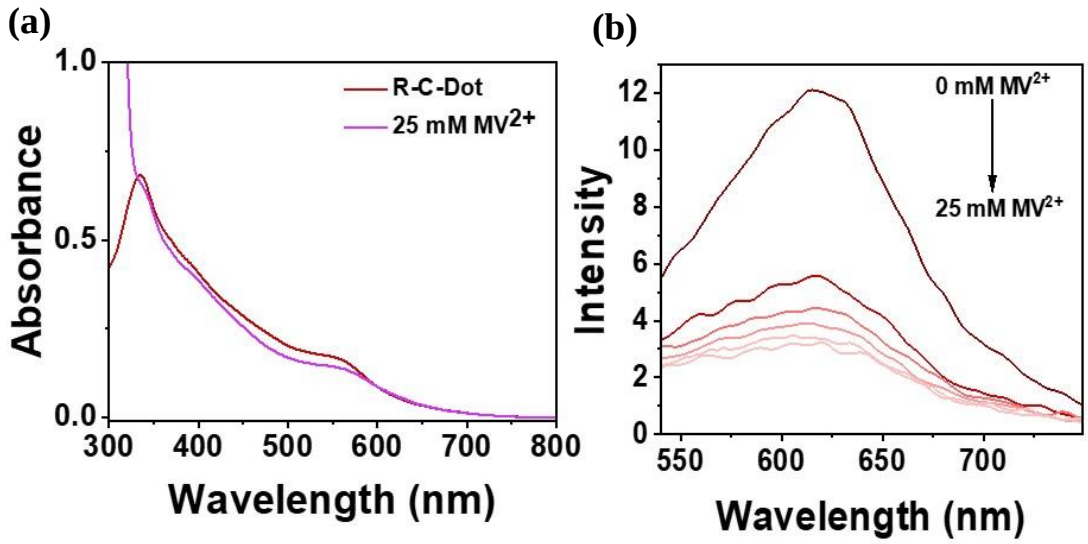

Figure S12: Steady state (a) absorbance (b) PL measurement of R-C-Dots in the presence of different concentrations of MV^{2+}.

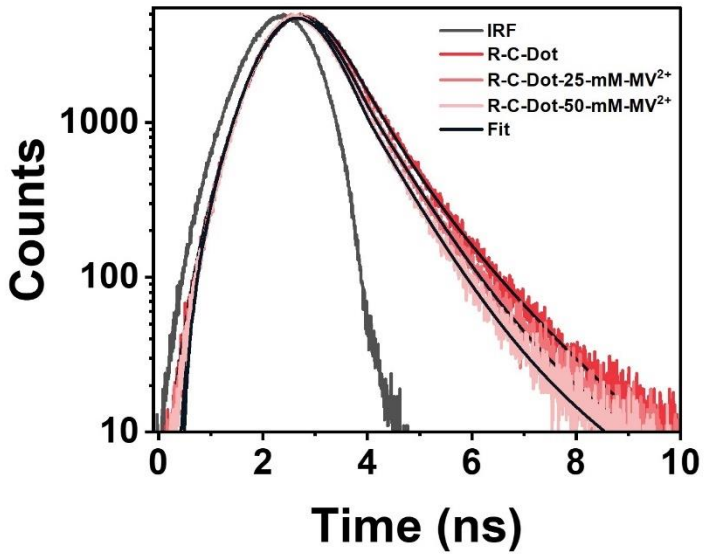

Figure S13: Time resolved fluorescence quenching analysis of R-C-Dots in the presence of different concentrations of MV^{2+} after the excitation at 605 nm and emission monitored at 650 nm.

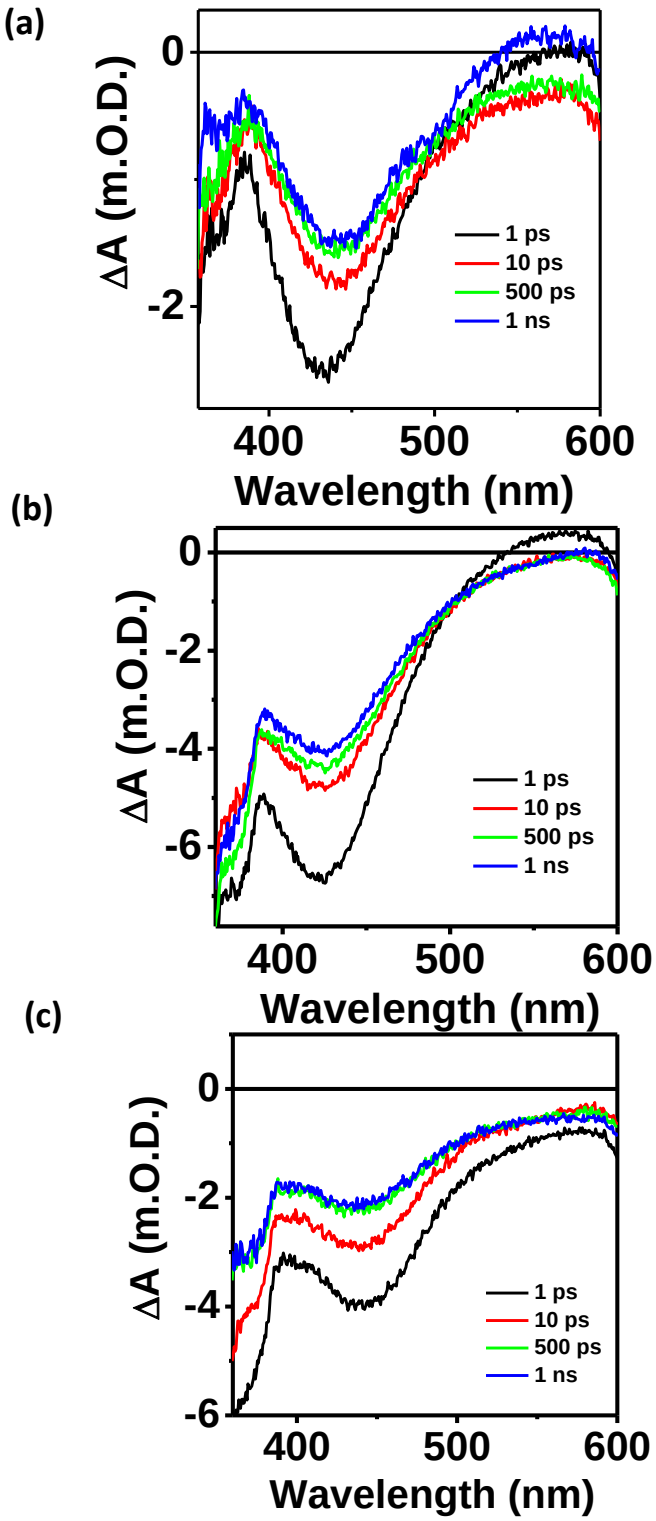

Figure S14: Transient absorption data of (a) B-C-Dots (b) G-C-Dots (c) R-C-Dots at different time delay after 320 nm excitation.

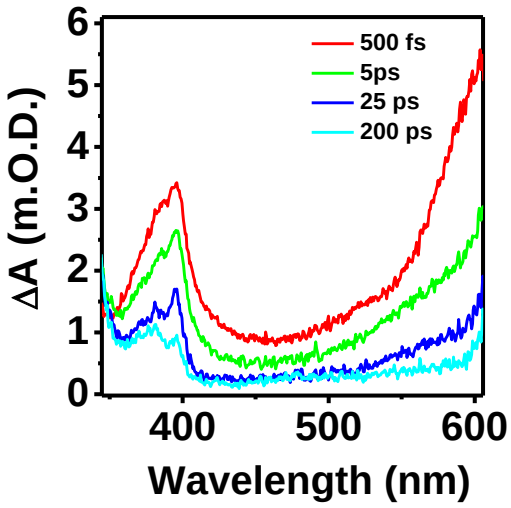

Figure S15: Transient absorption data of MV^{2+} at a different time delay after 320 nm excitation.

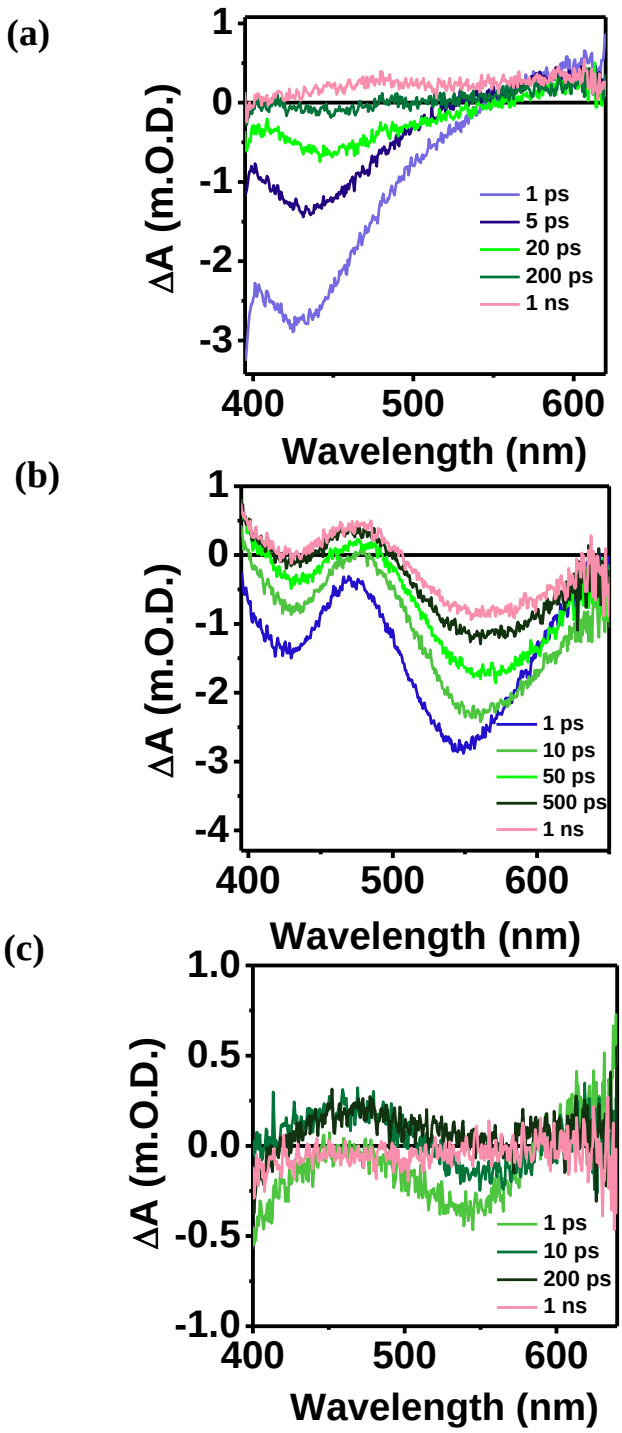

Figure S16: Transient absorption data of (a) B-C-Dots (b) G-C-Dots (c) R-C-Dots in the presence of MV^{2+} at different time delay after 380 nm excitation.

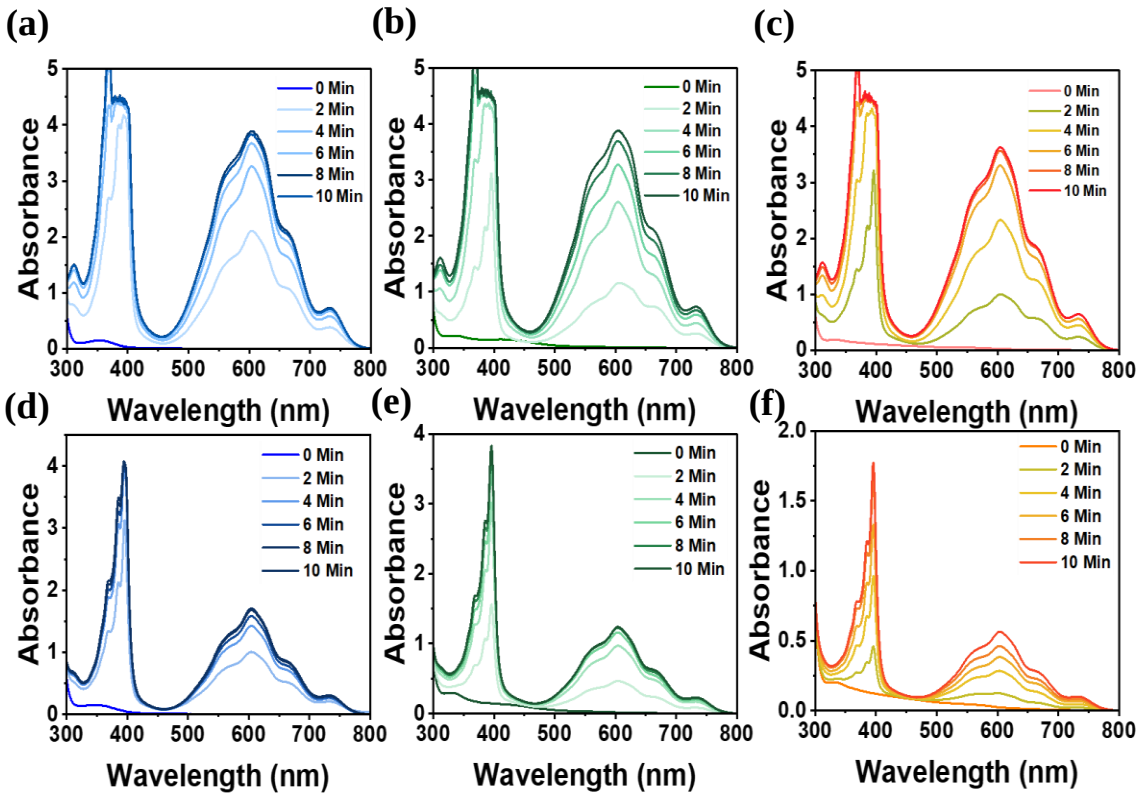

Figure S17: Absorbance spectrum of MV^{+2} radical generation study in different time intervals in the presence of (a) B-C-Dot, (b) G-C-Dot, and (c) R-C-Dot after the irradiation of UV light (top panel) and (d) B-C-Dot (e) G-C-Dot (f) R-C-Dot after irradiation of Visible light (bottom panel) in presence of sacrificial electron donor TEOA, respectively.

Table S1: Calculated percentage of elemental present in the different C-Dot.

Sample	C (%)	O (%)	N (%)
B-C-Dot	75.24	11.69	13.07
G-C-Dot	68.55	19.67	11.78
R-C-Dot	64.58	22.86	12.86

Table S2: Estimated band positions for surface and core from the cyclic voltammetry oxidation potential of various C-Dots.

Samples	E_{ox} (V)	VB (eV)	Core state Optical Band Gap ($E_{g, core}$) (eV)	Surface state Optical Bandgap ($E_{g, surf.}$) (eV)	Calculated Core State CB (eV)	Calculated surface state CB (eV)
B-C-Dot	1.31	-6.06	3.04	-	-3.02	
G- C-Dot	1.21	-5.96	2.66	2.15	-3.3	-3.81
R- C-Dot	1.05	-5.8	2.17	1.85	-3.63	-3.95

Table S3: Percentage of PL quenching at 440 nm and 530 nm of different emitting C-Dots after addition of 10 mM MV^{2+} after exciting at 340 nm and 530 nm respectively in water, DMSO, and DMF.

Samples	**λ_{ex}=340 nm, λ_{em}=440 nm (% of quenching)**	**λ_{ex}=420 nm, λ_{em}=530 nm (% of quenching)**
	Solvent: Water	
B-C-Dots	28	25
G-C-Dots	38	35
R-C-Dots	52	33
	Solvent: DMSO	
B-C-Dots	99	20
G-C-Dots	99	45
R-C-Dots	99	30
	Solvent: DMF	
B-C-Dots	90	23
G-C-Dots	96	52
R-C-Dots	96	60

Table S4: Time constants of time resolved PL quenching analysis for B-C Dots using 340 nm excitation light and emission monitored at 440 nm with different concentrations of MV^{2+}.

MV^{2+} (mM)	τ_1 (ns)	B_1 (%)	τ_2 (ns)	B_2 (%)	$<\tau>$ (ns)	χ^2
0	1.42	56.14	8.35	43.87	4.31	1.10
5	1.32	57.85	6.83	42.15	3.49	1.11
10	1.25	59.37	5.94	40.62	3.01	1.12
15	1.20	61.39	5.26	38.61	2.62	1.04
20	1.14	63.50	4.77	37.49	2.35	1.04
25	1.12	64.69	4.36	35.31	2.10	1.16

Table S5: Time constants of time resolved PL quenching analysis for G-C Dots using 340 nm excitation light and emission monitored at 440 nm with different concentrations of MV^{2+}.

MV^{2+} (mM)	τ_1 (ns)	B_1 (%)	τ_2 (ns)	B_2 (%)	$<\tau>$ (ns)	χ^2
0	2.04	26.70	9.56	73.3	7.46	1.20
5	1.46	26.40	6.77	73.59	5.29	1.10
10	1.25	28.11	5.51	71.89	4.24	1.11
15	1.23	32.02	4.82	67.97	3.58	1.14
20	1.17	35.00	4.26	65.00	3.09	1.15
25	0.94	33.17	3.68	66.82	2.69	1.19

Table S6: Time constants of time resolved PL quenching analysis for R-C Dots using 340 nm excitation light and emission monitored at 440 nm with different concentrations of MV^{2+}.

MV^{2+} (mM)	τ_1 (ns)	B_1 (%)	τ_2 (ns)	B_2 (%)	$<\tau>$ (ns)	χ^2
0	2.10	33.33	9.21	66.68	6.70	1.22
5	1.25	31.47	5.99	68.53	4.42	1.14
10	1.06	33.81	4.82	66.18	3.47	1.14
15	0.95	36.10	4.12	63.87	2.90	1.16
20	0.89	37.46	3.62	62.54	2.52	1.11
25	0.80	38.63	3.26	61.37	2.24	1.29

Table S7: Time constants of time resolved PL quenching analysis for B-C Dots using 405 nm excitation light and emission monitored at 530 nm with different concentrations of MV^{2+}.

MV^{2+} (mM)	τ_1 (ns)	B_1 (%)	τ_2 (ns)	B_2 (%)	$<\tau>$ (ns)	χ^2
0	1.62	26.88	6.12	73.12	4.86	1.12
5	1.48	29.25	5.39	70.75	4.19	1.14
10	1.43	29.82	4.82	70.18	3.75	1.12
15	1.33	30.67	4.34	69.33	3.35	1.09
20	1.23	31.08	3.95	68.92	3.04	1.05
25	1.22	32.94	3.71	67.06	2.83	1.09

Table S8: Time constants of time resolved PL quenching analysis for G-C Dots using 405 nm excitation light and emission monitored at 530 nm with different concentrations of MV^{2+}.

MV^{2+} (mM)	τ_1 (ns)	B_1 (%)	τ_2 (ns)	B_2 (%)	$\langle\tau\rangle$ (ns)	χ^2
0	0.17	2.07	5.37	97.93	5.26	1.14
5	0.56	4.41	4.80	95.59	4.61	1.14
10	1.37	12.76	4.76	87.24	4.32	1.15
15	1.26	13.95	4.61	86.05	4.14	1.16
20	1.34	16.35	4.55	83.65	4.02	1.16
25	1.34	18.61	4.51	81.39	3.92	1.17

Table S9: Time constants of time resolved PL quenching analysis for R-C Dots using 405 nm excitation light and emission monitored at 530 nm with different concentrations of MV^{2+}.

MV^{2+} (mM)	τ_1 (ns)	B_1 (%)	τ_2 (ns)	B_2 (%)	$\langle\tau\rangle$ (ns)	χ^2
0	0.97	10.65	6.16	89.35	5.61	1.17
5	1.01	10.04	5.79	89.96	5.31	1.16
10	0.86	8.27	5.66	91.73	5.26	1.15
15	0.85	8	5.56	92	5.19	1.14
20	0.86	8.11	5.46	91.89	5.09	1.16
25	0.84	7.67	5.27	92.33	4.93	1.15

References

1 N. Ghorai, S. Bhunia, S. Burai, H. N. Ghosh, P. Purkayastha, and S. Mondal, *Nanoscale*, 2022, **14**, 15812.

2 K. Holá, M. Sudolská, S. Kalytchuk, D. Nachtigallová, A. L. Rogach, M. Otyepka and R. Zbořil, *ACS Nano*, 2017, **11**, 12402.

3 B. Jana, Y. Reva, T. Scharl, V. Strauss, A. Cadranel and D. M. Guldi, *J. Am. Chem. Soc.*, 2021, **143**, 20122.4

4. T. Watanabe' and K. Honda, *J. Phys. Chem.*,1982, **86**, 2617.